Molecular Biology of the Cell
Vol. 16, 3987–3998, September 2005

Targeting of Tsc13p to Nucleus–Vacuole Junctions: A Role for Very-Long-Chain Fatty Acids in the Biogenesis of Microautophagic Vesicles

Erik Kvam,* Kenneth Gable,† Teresa M. Dunn,† and David S. Goldfarb*

*Department of Biology, University of Rochester, Rochester, NY 14627; and †Department of Biochemistry, Uniformed Services University of the Health Sciences, Bethesda, MD 20184

Submitted April 8, 2005; Revised May 25, 2005; Accepted June 6, 2005
Monitoring Editor: Peter Walter

***TSC13* is required for the biosynthesis of very-long-chain fatty acids (VLCFAs) in yeast. Tsc13p is a polytopic endoplasmic reticulum (ER) membrane protein that accumulates at nucleus–vacuole (NV) junctions, which are formed through Velcro-like interactions between Nvj1p in the perinuclear ER and Vac8p on the vacuole membrane. NV junctions mediate piecemeal microautophagy of the nucleus (PMN), during which bleb-like portions of the nucleus are extruded into invaginations of the vacuole membrane and degraded in the vacuole lumen. We report that Tsc13p is sequestered into NV junctions from the peripheral ER through Vac8p-independent interactions with Nvj1p. During nutrient limitation, Tsc13p is incorporated into PMN vesicles in an Nvj1p-dependent manner. The lumenal diameters of PMN blebs and vesicles are significantly reduced in *tsc13-1* and *tsc13-1 elo3-*Δ mutant cells. PMN structures are also smaller in cells treated with cerulenin, an inhibitor of de novo fatty acid synthesis and elongation. The targeting of Tsc13p-GFP into NV junctions is perturbed by cerulenin, suggesting that its binding to Nvj1p depends on the availability of fatty acid substrates. These results indicate that Nvj1p retains and compartmentalizes Tsc13p at NV junctions and that VLCFAs contribute to the normal biogenesis of trilaminar PMN structures in yeast.**

INTRODUCTION

The endoplasmic reticulum (ER) is a mosaic of dynamic subdomains, including those involved in interorganelle "contact sites" or zones of close apposition between the ER membrane and other subcellular compartments (reviewed in Voeltz *et al*. [2002] and Levine [2004]). Such contact sites have been observed between the ER and Golgi, mitochondrial, vacuolar (lysosomal), peroxisomal, endosomal, lipid droplet, or plasma membranes (Staehelin, 1997; Voeltz *et al*., 2002). ER contact sites have been proposed to mediate the nonvesicular trafficking of small molecules and lipids (reviewed in Levine, 2004). For example, mitochondria-associated ER membrane domains are implicated in the transport of phospholipids and sterols to and from mitochondria (Rusinol *et al*., 1994; Achleitner *et al*., 1999). Plasma membrane-associated ER subdomains may likewise facilitate the transfer of specific lipids to the plasma membrane (Pichler *et al*., 2001). Accordingly, mitochondrial and plasma membrane-associated ER domains are enriched in enzymes involved in the biosynthesis of phospholipids and sterols (Rusinol *et al*., 1994; Gaigg *et al*., 1995; Stone and Vance, 2000; Pichler *et al*., 2001).

The structural basis for the establishment and maintenance of ER contact sites in eukaryotes is largely unknown, except in the case of nucleus–vacuole (NV) junctions in *Saccharomyces cerevisiae* (Pan *et al*., 2000; Voeltz *et al*., 2002; Levine, 2004). NV junctions occur where the vacuolar membrane protein Vac8p associates with Nvj1p in the outer nuclear membrane that is continuous with the perinuclear ER in yeast (Pan *et al*., 2000). The sizes of NV junctions increase proportionally to the expression level of Nvj1p, which is up-regulated though nutrient depletion following the diauxic shift or acute carbon or nitrogen starvation (Gasch *et al*., 2000; Roberts *et al*., 2003). The upstream promoter region of *NVJ1* contains stress response elements that control expression in response to nutrient stress (Moskvina *et al*., 1998). NV junctions are sites of piecemeal microautophagy of the nucleus (PMN), during which nonessential portions of the nucleus are pinched off into invaginations of the vacuole membrane and subsequently degraded by hydrolytic enzymes in the vacuole lumen (Roberts *et al*., 2003). PMN occurs at low frequencies in rapidly dividing cells, but it is induced to higher levels upon carbon or nitrogen starvation through the TOR nutrient response pathway (Roberts *et al*., 2003). The granular nucleolus, which is composed largely of preribosomes, is one nonessential nuclear constituent that has been observed to partition into PMN blebs (Roberts *et al*., 2003).

Recently, two conserved proteins with roles in lipid metabolism, namely, Tsc13p and Osh1p, were shown to localize at NV junctions (Kohlwein *et al*., 2001; Levine and Munro, 2001). Osh1p belongs to a family of proteins related to mammalian oxysterol binding protein (OSBP), which participates in the regulation of sterol homeostasis (Levine and

This article was published online ahead of print in *MBC in Press* (http://www.molbiolcell.org/cgi/doi/10.1091/mbc.E05–04–0290) on June 15, 2005.

Address correspondence to: David S. Goldfarb (dasg@mail.rochester.edu).

Abbreviations used: ER, endoplasmic reticulum; EYFP, enhanced yellow fluorescent protein; FAS, fatty acid synthase; GFP, green fluorescent protein; NV, nucleus–vacuole; PMN, piecemeal microautophagy of the nucleus; VLCFA, very-long-chain fatty acid; wt, wild-type.

Table 1. Strains used in this study

Strain	Genotype	Source
BY4741**a**	*MAT***a** *his3-Δ1 leu2-Δ met15-Δ ura3-Δ*	Euroscarf #Y00000
BY4741**a** *atg7Δ::kanMX4*	*MAT***a** *his3-Δ1 leu2-Δ met15-Δ ura3-Δ YHR171w::kanMX4*	Euroscarf #Y07090
FY1679α	*MATα ura3–52 leu2Δ1 trp1Δ63 his2Δ200*	Kohlwein *et al.* (2001)
FY1679α *cTSC13-EGFP*	*MATα ura3-52 leu2Δ1 YDL015c-EGFP-kanMX6*	Kohlwein *et al.* (2001)
FY1679α *cELO3-EGFP*	*MATα ura3-52 leu2Δ1 trp1Δ63 YLR372w-EGFP-kanMX6*	Kohlwein *et al.* (2001)
FY1679**a** *cYBR159-EGFP*	*MAT***a** *ura3-52 YBR159w-EGFP-kanMX6*	Han *et al.* (2002)
TDY2037	*MATα ura3-52 leu2-Δ trp1-Δ lys2*	Kohlwein *et al.* (2001)
TDY2051 *tsc13-1*	*MATα ura3-52 leu2-Δ trp1-Δ lys2 ade2-101 tsc13-1*	Kohlwein *et al.* (2001)
TDY2058 *tsc13-1 elo3-Δ*	*MATα ura3-52 leu2-Δ trp1-Δ lys2 ade2-101 tsc13-1 YLR372w::TRP1*	Kohlwein *et al.* (2001)
YEF473**a**	*MAT***a** *trp1-Δ63 leu2-Δ1 ura3–52 his3-Δ200 lys2-801*	Bi and Pringle (1996)
YEF473α	*MATα trp1-Δ63 leu2-Δ1 ura3-52 his3-Δ200 lys2-801*	Bi and Pringle (1996)
YEF473**a** *nvj1Δ::kan^r*	*MAT***a** *trp1-Δ63 leu2-Δ1 ura3-52 his3-Δ200 lys2-801 YHR195w::kan^r*	Pan *et al.* (2000)
YEF473α *vac8Δ::kan^r*	*MATα trp1-Δ63 leu2-Δ1 ura3-52 his3-Δ200 lys2-801 YEL013w::kan^r*	Pan *et al.* (1998)
YEF473**a** *cNVJ1-EYFP*	*MAT***a** *trp1-Δ63 leu2-Δ1 ura3-52 his3-Δ200 lys2-801 YHR195w-EYFP-kan^r*	Pan *et al.* (2000)

Munro, 2001). Osh1p and related OSBP family members are hypothesized to function in the nonvesicular transport of sterol lipids between membrane compartments (reviewed in Levine, 2004). In support of this model, mammalian CERT, which shares a similar domain structure to Osh1p, has been shown to extract and transfer ceramide from the ER to nearby Golgi membranes (Hanada *et al.*, 2003; Kumagai *et al.*, 2005). We recently showed that Osh1p is sequestered into NV junctions through direct, Vac8p-independent interactions with Nvj1p and that a redundant function of the *OSH1–7* family of proteins is required for efficient PMN (Kvam and Goldfarb, 2004).

Tsc13p is an essential protein required for the elongation of long-chain fatty acids (C_{16} and C_{18}) to very-long-chain fatty acids (VLCFAs), which possess acyl-chain lengths of 20 carbons or more (Kohlwein *et al.*, 2001). VLCFAs are constituents of several complex lipid species in yeast, including ceramides, sphingolipids, inositolglycerophospholipids, and the phosphatidylinositol moiety of GPI anchors (Dickson, 1998), each of which are important components of lipid rafts and other detergent-insoluble lipid microdomains (Eisenkolb *et al.*, 2002; Dupre and Haguenauer-Tsapis, 2003; Boukh-Viner *et al.*, 2005). Accordingly, various studies indicate that VLCFAs strongly influence the structure, function, and fluidity of biological membranes (Ho *et al.*, 1995; Schneiter *et al.*, 1996; Millar *et al.*, 1998).

VLCFA biosynthesis in yeast occurs through a microsomal fatty acid elongation cycle that partially overlaps with the activity of the soluble fatty acid synthase (FAS) complex (Rossler *et al.*, 2003). During VLCFA elongation, 2-carbon units from malonyl CoA are sequentially condensed onto C_{16}/C_{18} long-chain fatty acyl-CoA precursors, thereby increasing the acyl chain length of the fatty acid substrate (Schneiter and Kohlwein, 1997; Kohlwein *et al.*, 2001). C_{26} is the most abundant VLCFA produced in this manner in yeast (Welch and Burlingame, 1973). One round of elongation requires four consecutive biochemical reactions that are catalyzed by Elo2p, Elo3p, Tsc13p, and Ybr159p (Rossler *et al.*, 2003). Elo2p and Elo3p are related elongases with partially overlapping fatty acyl-CoA substrate specificities, and thus they form two separate elongase systems (Oh *et al.*, 1997; Rossler *et al.*, 2003). Copurification studies indicate that Tsc13p and Ybr159p may associate in distinct elongase complexes with either Elo2p or Elo3p (Kohlwein *et al.*, 2001; Han *et al.*, 2002). Based on mutant phenotypes in yeast, and sequence similarity to reductases in higher eukaryotes, Tsc13p is thought to be the enoyl-CoA reductase that catalyzes the final step of VLCFA formation (Kohlwein *et al.*, 2001; Gable *et al.*, 2004).

Here, we show that the activity of Tsc13p in the VLCFA elongation cycle contributes to the biogenesis of PMN blebs and vesicles in yeast. This role is directly facilitated by the selective targeting of Tsc13p to NV junctions through a physical association with Nvj1p. The Nvj1p-mediated targeting of Tsc13p to NV junctions and the incorporation of Tsc13p into PMN structures provide a unique opportunity to investigate the interplay between the structure and function of a model ER membrane contact site.

MATERIALS AND METHODS

Yeast Strains, Plasmids, and Growth Conditions

Yeast strains used in this study are listed in Table 1. Plasmids for the expression of *NVJ1*, *NVJ1-EYFP*, and *NVJ1-Fc* under *CUP1* promoter control (P_{CUP1}-*NVJ1*, P_{CUP1}-*NVJ1-EYFP*, and P_{CUP1}-*NVJ1-Fc*) or *NVJ1-myc* under *GAL1* promoter control (P_{GAL1}-*NVJ1-myc*) were described previously (Pan *et al.*, 2000; Roberts *et al.*, 2003; Kvam and Goldfarb, 2004). P_{CUP1}-*TSC13-EYFP* was created by ligating a *Sma*I-*TSC13*-*Hind*III PCR fragment and a *Hind*III-*EYFP*-*Xho*I PCR fragment into the *Sma*I and *Sal*I sites of pJN40 (Macreadie *et al.*, 1989; Pan *et al.*, 2000). PCR fragments were amplified from genomic yeast DNA or pEYFP (BD Biosciences Clontech, Palo Alto, CA) using *Taq*DNA polymerase (Invitrogen, Carlsbad, CA). Construction of pRS425-*TSC13*, encoding *TSC13* under the control of its native promoter, was described previously (Kohlwein *et al.*, 2001). Plasmids for the expression of Elo2p-enhanced green fluorescent protein (EGFP) (pUG35-*ELO2-EGFP*) were generously obtained from S. Kohlwein (University of Graz, Graz, Austria). The plasmid-based *VAC8* myristoylation and palmitoylation double mutant (*vac8-4*) was obtained from L. Weisman (University of Iowa, Iowa City, IA) (Wang *et al.*, 1998). Unless otherwise indicated, cells were cultured in standard YPD or synthetic complete media (SC) with 2% glucose (SCGlu) at 30°C (Sherman, 1991). Nitrogen starvation media (SD-N) contained 0.17% yeast nitrogen base and 2% glucose without amino acids or ammonium sulfate. The antibiotic cerulenin (Sigma, St. Louis, MO) was dissolved in ethanol and used at a final concentration of 45 μM. Myriocin (ISP-1; Sigma) was suspended in methanol and used at 1 μg/ml. Where indicated, myristic acid (Sigma) was supplemented to media at a final concentration of 1 mM from a 100 mM stock in ethanol. To disperse myristic acid, 0.2% Tergitol (Type NP-40; Sigma) was added to the media.

In Vivo Nvj1p-Fc Copurification

Yeast harboring P_{CUP1}-*TSC13-EYFP* and either P_{CUP1}-*NVJ1-Fc* or empty vector, respectively, were grown to log phase in 100 ml of SCGlu and induced for 3 h with 0.1 mM $CuSO_4$. Nvj1p-Fc was isolated from whole cell extract using protein A-conjugated agarose as described previously (Kvam and Goldfarb, 2004). Nvj1p-Fc complexes were denatured from the agarose matrix with 40 μl of 2× sample loading buffer (100 mM Tris-HCl, pH 6.8, 2% SDS, 20% glycerol, 0.1% bromphenol blue, and 2% 2-mercaptoethanol) and boiled for 5 min. Then, 10–20 μl of eluate was analyzed by SDS-PAGE, and the copurification of Tsc13p-EYFP was assessed by immunoblot.

Vac8p Fractionation

Approximately 25 OD_{600} units of log phase cells expressing cTsc13p-EGFP were shifted into 50 ml of SD-N media supplemented with either cerulenin or an equal volume of ethanol (mock treatment). Cells were starved overnight (~16 h) at 30°C and then harvested. Whole cell extracts were prepared by bead-beating in extraction buffer (0.3 M sorbitol, 10 mM Tris-Cl, pH 7.5, 0.1 M NaCl, 1 mM $MgCl_2$, and 1 mM EDTA) containing Complete protease inhibitors (Roche Diagnostics, Mannheim, Germany) and 1 mM phenylmethylsulfonyl fluoride. Extracts were precleared by centrifugation (2000 rpm × 10 min), and the resulting lysate was fractionated by differential centrifugation as described by Wang *et al*., 1998. Briefly, precleared lysates were centrifuged at 13,000 × *g* for 10 min and separated into P13 pellet and S13 supernatant fractions. S13 fractions were then separated into P100 pellet and S100 supernatant fractions by ultracentrifugation (100,000 × *g* for 30 min). Pelleted membranes in P13 and P100 fractions were solubilized in extraction buffer containing 1% NP-40 detergent and protease inhibitors. The protein content of each P13, S100, and P100 fraction was determined using Bradford reagent. Equal amounts of protein were mixed with 2× sample loading buffer, boiled for 5 min, and separated by SDS-PAGE. Vac8p was probed in each fraction by immunoblot and compared with the fractionation profile of *vac8-4* cells that were starved and processed in a similar manner.

Fatty Acid Analysis

Cells expressing cTsc13p-EGFP were grown in YPD to ~1.0 OD_{600}, at which time they were transferred into SD-N media containing cerulenin or an equal amount of ethanol (mock treatment) to an OD_{600} of 0.5 and then starved for 24 h in the presence or absence of myristic acid. Fatty acid methyl esters (FAMEs) were extracted from 2 OD_{600} units of cells by acid methanolysis as described previously (Kohlwein *et al*., 2001). Briefly, cells were treated with 1 M methanolic HCl for 40 min at 78°C and then extracted into hexane:ether (1:1). FAMEs were dried, dissolved in hexane, and separated on an Agilent GC 6890 using a Hewlett Packard INNOWax column at constant flow (0.5 ml/min). The oven was ramped from 90°C to 250°C at 40°C/min and held at 250°C for 90 min. FAMEs were detected using an Agilent MS 5973. Internal C_{21} (heneicosanoic) and C_{23} (tricosanoic) fatty acid standards, added to the cells before extraction, were used to normalize the data. The percentage of each fatty acid species was calculated from the sum of each FAME peak value and averaged among three independent experiments.

Immunoblotting

Unless otherwise indicated, protein extracts were prepared by trichloroacetic acid (TCA) precipitation as described previously (Roberts *et al*., 2003). Tsc13p-EYFP and cTsc13p-EGFP were probed by immunoblot with polyclonal BD Living Colors Av peptide green fluorescent protein (GFP) antibodies (BD Biosciences Clontech). Nvj1p-myc was probed using mouse anti-c-Myc monoclonal antibody (Zymed Laboratories, South San Francisco, CA). Vac8p was probed with polyclonal antibodies raised against purified Vac8p (Pan *et al*., 2000). Nvj1p and Nvj1p-Fc were probed with polyclonal antibodies raised against a segment of Nvj1p (Kvam and Goldfarb, 2004). All immunoprobed proteins were detected with either horseradish peroxidase-coupled donkey anti-rabbit antibody (Santa Cruz Biotechnology, Santa Cruz, CA) or horseradish peroxidase-coupled goat anti-mouse antibody (Santa Cruz Biotechnology) where appropriate and developed by chemiluminescence using Luminol Reagent (Santa Cruz Biotechnology).

Quantitative Degradation Analysis of Nvj1p-myc and cTsc13p-EGFP

Cells expressing cTsc13p-EGFP were grown in YPD to log phase (~1 OD_{600}), washed, and shifted into starvation media to an OD_{600} of 0.5. Cells harboring P_{GAL1}-*NVJ1-myc* were grown, induced, and shifted into SD-N starvation media in a manner analogous to previously published degradation analyses of Nvj1p (Roberts *et al*., 2003). Cerulenin was applied to SD-N media at a final concentration of 45 μM, and control cells were treated with an equivalent volume of ethanol. Two OD units of culture were then collected immediately (zero point) and equivalent volumes of culture were harvested after 10 and 20 h of starvation, respectively. Protein extracts were prepared by TCA precipitation as described previously (Roberts *et al*., 2003). Samples were separated by SDS-PAGE and immunoprobed as indicated.

Cell Imaging

Cells were grown in YPD or SCGlu to the indicated OD_{600} with or without induction of specific reporters. Elo2p-EGFP expression was induced in cells harboring pUG35-*ELO2-EGFP* by culturing in medium lacking methionine for 1.5 h. For P_{CUP1}-*TSC13-EYFP*, P_{CUP1}-*NVJ1*, and P_{CUP1}-*NVJ1-Fc*, high levels of expression were obtained by fortifying media with 0.1 mM $CuSO_4$ for the times indicated, whereas basal levels of expression were achieved by withholding $CuSO_4$. For all experiments using SD-N starvation media, $CuSO_4$ was withheld due to the positive feedback of nitrogen starvation on the *CUP1* promoter (Gasch *et al*., 2000). Vacuoles were stained with FM4-64 in rich medium as described previously (Pan and Goldfarb, 1998). In cells starved of nitrogen (SD-N), vacuoles were first stained with FM4-64 in rich media, and then the cells were washed three times with SD-N and starved for the times indicated. For overnight starvation experiments, the localization of cNvj1p-EYFP or cTsc13p-EGFP was analyzed from SCGlu overnight starter cultures after ~15 h of starvation (SD-N) in the presence of cerulenin, myriocin, or equivalent amounts of ethanol, with or without myristic acid. DNA was stained immediately before microscopic analysis with 5 M Hoechst reagent H-1398 (Molecular Probes, Eugene, OR).

Confocal Microscopy

Confocal microscopy was performed on a Leica TCS NT microscope equipped with a 100× Fluorotar lens and UV, Ar, Kr/Ar, and He/Ne lasers (Leica Microsystems, Chantilly, VA). Laser power and photomultiplier tube settings were kept constant for all experiments unless otherwise indicated. PMN morphology was digitally analyzed using the Profile function of the Leica Confocal Software package (Version 2.5, Build 1227), which reports the pixel profile and length of a line segment applied to an image. PMN structures were captured by scanning the Z-axis of the cell for the section that yielded the largest surface area of colocalization between Nvj1p-GFP and FM4-64 labeled vacuole membranes. Line segments were drawn across the lumen of the largest representative PMN structures, starting from the nucleus–vacuole interface and ending at the opposing face of the PMN structure, in a manner that approximately bisected the nuclear PMN bleb or vesicle. The boundaries of each line segment were determined in part by the pixel intensity of Nvj1p-EYFP and/or FM4-64 along the measured section as well as a visual fit. All images were processed using Adobe PhotoShop 5.0 (Adobe Systems, Mountain View, CA).

RESULTS

Peripheral and Perinuclear ER Pools of Tsc13p Are Targeted to NV Junctions Proportional to Nvj1p Levels

Tsc13p is an integral membrane protein of the ER network that accumulates at interfaces between nuclear and vacuolar membranes called NV junctions (Pan *et al*., 2000; Kohlwein *et al*., 2001). The intensity of GFP-labeled Tsc13p at NV junctions reportedly increases as cells approach stationary phase (Kohlwein *et al*., 2001). This phenomenon is reminiscent of the Nvj1p-mediated recruitment of Osh1p to NV junctions from soluble and Golgi-associated pools during stationary phase or nitrogen starvation (Levine and Munro, 2001; Kvam and Goldfarb, 2004). NV junctions normally expand and proliferate in response to the nutrient stress-related up-regulation of *NVJ1* (Roberts *et al*., 2003). Thus, we investigated the possibility that Nvj1p might target Tsc13p to NV junctions in a manner analogous to Osh1p.

We first examined the localization of an integrated cTsc13p-EGFP chimera (expressed from the *TSC13* chromosomal locus) as a function of Nvj1p expression. Cells expressing cTsc13p-EGFP were monitored by confocal microscopy during early log phase when physiological levels of Nvj1p are very low (Pan *et al*., 2000; Roberts *et al*., 2003). Under these conditions, only a small proportion of the cellular pool of microsomal cTsc13-EGFP colocalized with FM4-64 stained vacuolar membranes to produce the yellow fluorescence characteristic of NV junctions, whereas the remaining pool localized throughout the peripheral and perinuclear ER (Figure 1A, i and ii). The incremental induction of plasmid-encoded Nvj1p (P_{CUP1}-*NVJ1*) in these cells resulted in proportional increases in the amount and intensity of cTsc13-EGFP at NV junctions (Figure 1A, iii and iv, v and vi). Virtually the entire cellular pool of cTsc13p-EGFP localized to NV junctions in cells expressing high levels of Nvj1p, apparently at the expense of peripheral and perinuclear ER pools (Figure 1A, v and vi). Only very low levels of cTsc13p-EGFP fluorescence could be detected in peripheral ER membranes within these cells at higher confocal laser settings (our unpublished data). By Western blot, the overexpression of *NVJ1* had no affect on cTsc13p-EGFP protein levels (Figure 1B), consistent with the notion that preexisting pools of cTsc13p-EGFP were reapportioned into NV junctions from

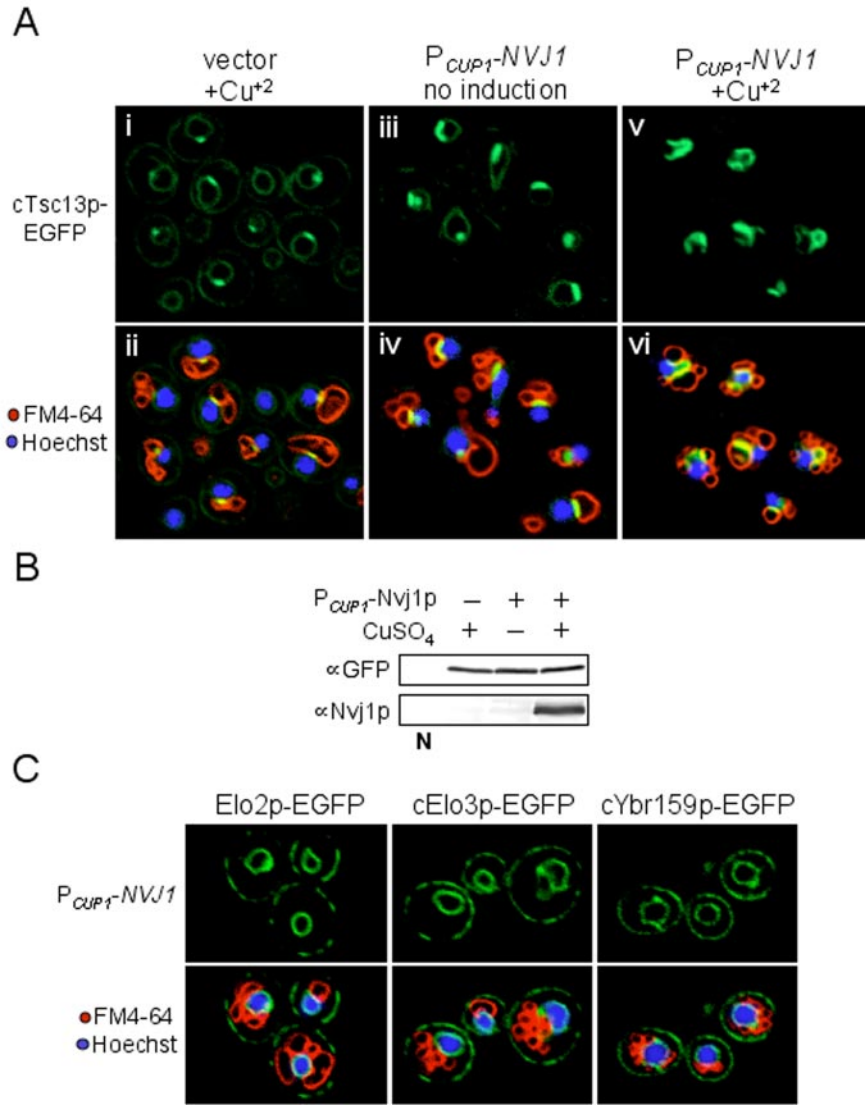

Figure 1. Tsc13p is sequestered from peripheral and nuclear ER pools to NV junctions in an Nvj1p-dependent manner. (A) Localization of chromosomally expressed cTsc13p-EGFP as a function of *NVJ1* induction. Cells expressing cTsc13p-EGFP and harboring either P_{CUP1}-*NVJ1* or empty vector were analyzed at low OD_{600} (~0.3). P_{CUP1}-*NVJ1* expression was maintained at a basal level (iii and iv) or induced for 1.5 h with $CuSO_4$ (v and vi) similar to empty vector control cells (i and ii). Nuclear chromatin (blue) and vacuolar membranes (red) were costained with Hoechst and FM4-64, respectively. NV junctions look yellow in the overlay (bottom). The fluorescence of cTsc13p-EGFP decreases at peripheral ER pools (i) and perinuclear ER pools (iii) but increases at NV junctions (v and vi) as Nvj1p levels rise. (B) Immunoblot analysis of cTsc13p-EGFP protein levels in whole cell extract as a function of *NVJ1* expression. Wild-type extract lacking cTsc13p-EGFP denoted as N. (C) Associate ER proteins involved in VCLFA biosynthesis (Elo2p, Elo3p, and YBR159p) do not specifically accumulate at NV junctions when *NVJ1* is induced (nor are they excluded). Cells harboring P_{CUP1}-*NVJ1* and expressing chromosomally expressed cElo3p-EGFP, cYbr159p-EGFP, or plasmid-encoded Elo2p-EGFP were analyzed at log phase and stained for nuclear chromatin (blue) or vacuolar membranes (red) as described above.

the surrounding ER. Additionally, the induction of *NVJ1* failed to specifically target other ER membrane proteins involved in very-long-chain fatty acid synthesis (namely, Elo2p, Elo3p, and Ybr159p) to NV junctions (Figure 1C), although none of these factors were completely excluded from NV junctions. Thus, we conclude that NV junctions serve as high-affinity molecular sinks for microsomal pools of Tsc13p. Because NV junctions naturally proliferate in response to nutrient depletion, it is likely that the recruitment of Tsc13p to NV junctions in both postdiauxic (Kohlwein *et al*., 2001) and nutrient-starved (see below) cells is physiologically relevant to the cell's response to nutrient limitation.

Nvj1p Mediates the Localization of Tsc13p to Subdomains of the Perinuclear ER through Physical Association

To investigate whether Nvj1p plays a direct role in targeting Tsc13p to NV junctions, we next analyzed the ER distribution of Tsc13p in strains lacking either *NVJ1* or *VAC8*. Tsc13p-EYFP was cloned under the control of the *CUP1* promoter (P_{CUP1}-*TSC13-EYFP*) and induced with copper sulfate in wt, *nvj1*-Δ, and *vac8*-Δ cells (see *Materials and Methods*). In wild-type (wt) cells, Tsc13p-EYFP localized throughout the ER network but accumulated at small nuclear ER patches that colocalized with FM4-64 stained vacuoles, forming yellow-labeled NV junctions (Figure 2A, arrowheads). These yellow patches were absent in both *nvj1*-Δ and *vac8*-Δ cells, consistent with the loss of NV junctions (Figure 2B). Interestingly, Tsc13p-EYFP accumulated in large patches on the nuclear surface in *vac8*-Δ (*NVJ1*$^+$) cells (Figure 2B, arrowheads) whereas, in *nvj1*-Δ cells, it localized more homogeneously throughout the perinuclear ER (Figure 2B). These results indicated that Tsc13p might bind directly to Vac8p-independent patches of Nvj1p on the nuclear surface, which occur at low frequencies in *vac8*-Δ cells (Kvam and Goldfarb, 2004).

The possibility of a physical interaction between Nvj1p and Tsc13p was tested by affinity copurification using an Nvj1p reporter (Nvj1p-Fc) fused to the constant region of human IgG (Kvam and Goldfarb, 2004). Nvj1p-Fc expression efficiently rescued NV-junction formation in *nvj1*-Δ cells and targeted Tsc13p-EYFP to NV junctions from the surrounding ER (Figure 2C, i, arrowhead). Likewise, Tsc13p-EYFP biochemically copurified with Nvj1p-Fc in extracts of these cells (Figure 2D). In parallel control experiments, the pull-down of Tsc13p-EYFP was not detected in *nvj1*-Δ cell extracts

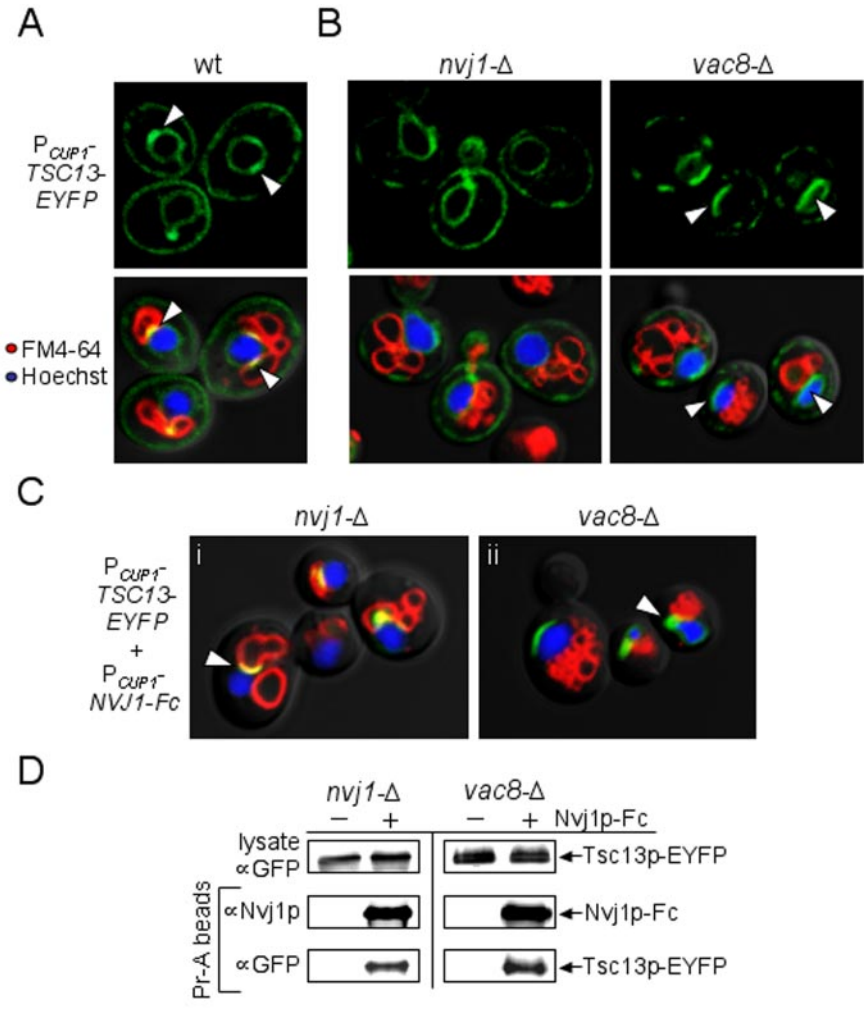

Figure 2. Tsc13p colocalizes and copurifies with Nvj1p in the perinuclear ER independent of Vac8p. (A) Plasmid-bound Tsc13p-EYFP expressed from the inducible *CUP1* promoter (P_{CUP1}-*TSC13-EYFP*) accumulates at NV junctions in wt cells. Vacuolar membranes (red) and nuclear chromatin (blue) were costained with FM4-64 and Hoechst, respectively. NV junctions (see arrows) look yellow in the overlay. (B) The accumulation of Tsc13p-EYFP at NV junctions is dependent on both Nvj1p and Vac8p. *nvj1*-Δ cells and *vac8*-Δ cells expressing P_{CUP1}-*TSC13-EYFP* were analyzed at log phase by confocal microscopy. Vacuolar membranes (red) and nuclear chromatin (blue) were costained as described above. Arrows point out the novel accumulation of Tsc13p-EYFP at patches in the perinuclear ER of *vac8*-Δ cells. (C) Overexpression of Nvj1p-Fc in *nvj1*-Δ cells restores the targeting of Tsc13p-EYFP to NV junctions and targets Tsc13p-EYFP to perinuclear ER patches in *vac8*-Δ cells. Log phase *nvj1*-Δ and *vac8*-Δ cells harboring both P_{CUP1}-*TSC13-EYFP* and P_{CUP1}-*NVJ1-Fc* were induced for 1.5 h with $CuSO_4$. Vacuolar membranes (red) and nuclear chromatin (blue) were stained as described above. NV junctions look yellow in the overlay (i, see arrow). Tsc13p-EYFP accumulates at nonyellow nuclear ER patches in *vac8*-Δ cells after Nvj1p-Fc induction (ii, see arrow). (D) Tsc13p-EYFP specifically copurifies with Nvj1p-Fc from *nvj1*-Δ and *vac8*-Δ cell extracts. Lysates of cells harboring P_{CUP1}-*TSC13-EYFP* and either P_{CUP1}-*NVJ1-Fc* or empty vector were prepared as described in *Materials and Methods*. Nvj1p-Fc complexes were purified using protein A-conjugated agarose beads. The copurification of Tsc13p-EYFP was assessed by immunoblot using polyclonal GFP antibodies.

lacking Nvj1p-Fc (Figure 2D), and Nvj1p-Fc showed no specific affinity for GFP alone (our unpublished data). The physical interaction between Nvj1p and Tsc13p proved to be independent of NV-junction formation, as Tsc13p-EYFP also copurified with Nvj1p-Fc from *vac8*-Δ cell extracts (Figure 2D). Consistent with this finding, the overexpression of Nvj1p-Fc in *vac8*-Δ cells triggered the relocalization of Tsc13p-EYFP from the peripheral ER to perinuclear ER clusters (Figure 2C, ii, arrowhead), presumably as a consequence of the clustering of Nvj1p-Fc on the nuclear surface in the absence of Vac8p (Pan *et al*., 2000; Kvam and Goldfarb, 2004). These results illustrate that Tsc13p can accumulate at perinuclear ER patches via direct or, less likely, indirect association with Nvj1p, irrespective of Vac8p and NV junction formation. We conclude that Nvj1p likely binds and sequesters Tsc13p into a subdomain of the perinuclear ER, similar in manner to Vac8p and Osh1p (Pan *et al*., 2000; Kvam and Goldfarb, 2004).

Tsc13p Accumulates in PMN Blebs and Vesicles during Nutrient Stress

Our results thus far demonstrate that Tsc13p is normally targeted to NV junctions by association with Nvj1p. Because NV junctions serve as platforms for the production of nuclear blebs and vesicles during PMN, we thought it likely that Tsc13p also might be incorporated into PMN structures and targeted to the vacuole lumen. To test this hypothesis, the localization of plasmid-encoded Tsc13p-EYFP was analyzed under conditions that promote PMN, namely, stationary phase and nitrogen starvation (Roberts *et al*., 2003). In cells grown to high density and shifted into nitrogen starvation medium (SD-N), Tsc13p-EYFP frequently colocalized with FM4-64 stained vacuole membranes at bleb-like structures protruding directly from NV junctions (Figure 3A, arrowheads). Less frequently, Tsc13p-EYFP also localized to vesicular structures in the vacuole lumen that displayed rapid Brownian motions similar to macro- and microautophagic vesicles (Figure 3A). To distinguish between macro- and microautophagic structures and to confirm that Tsc13p-EYFP localized specifically to PMN vesicles in the vacuole lumen, we analyzed the localization of Tsc13p-EYFP in *atg7*-Δ cells, which are completely defective in macroautophagy (Kim *et al*., 1999) but normal for PMN (Roberts *et al*., 2003). As shown in Figure 3B, Tsc13p-EYFP localized to bona fide PMN blebs and vesicles in starved *atg7*-Δ cells.

Tsc13p-EYFP labeling was never observed in PMN-like structures in starved *nvj1*-Δ cells, consistent with the loss of NV-junctions and PMN (our unpublished data). Therefore, we investigated the targeting of chromosomal-encoded cTsc13p-EGFP to PMN structures as a function of *NVJ1* expression. Under physiological levels of Nvj1p, cTsc13p-EGFP accumulated within very tiny PMN blebs and vesicles

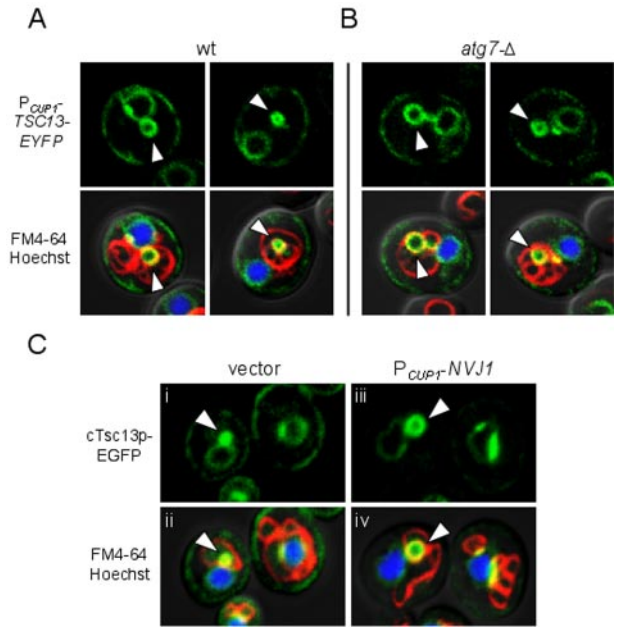

Figure 3. Tsc13p accumulates in nuclear PMN blebs and vesicles during stationary phase and nitrogen starvation. (A and B) Tsc13p-EYFP localizes to PMN blebs and vesicles in wt (A) and *atg7*-Δ (B) cells upon nitrogen starvation. Cells harboring P$_{CUP1}$-*TSC13-EYFP* were grown in SCGlu to stationary phase (~1.0 OD$_{600}$), shifted to SD-N medium, and analyzed by confocal microscopy after 3 h of starvation. Vacuolar membranes (red) and nuclear chromatin (blue) were stained with FM4-64 and Hoechst, respectively, and superimposed. Tsc13p-EYFP localizes to yellow-labeled PMN structures (see arrows) independent of *ATG7*. (C) Chromosomally expressed cTsc13p-EGFP increasingly accumulates in PMN structures proportional to *NVJ1* expression. Cells expressing cTsc13p-EGFP and harboring P$_{CUP1}$-*NVJ1* (iii and iv) or empty vector (i and ii) were grown to low OD$_{600}$ (~0.3), shifted to SD-N media, and analyzed by confocal microscopy after 3 h of starvation. Vacuolar membranes (red) and nuclear chromatin (blue) were stained as described above. PMN structures (see arrows) look yellow in the overlay and increase in size proportional to the targeting of cTsc13p-EGFP to NV junctions and *NVJ1* expression.

after a short incubation in SD-N (Figure 3C, i and ii). However, increased expression of plasmid-encoded *NVJ1* in these cells triggered the striking recruitment of cTsc13p-EGFP from the surrounding ER to enlarged PMN structures (Figure 3C, iii and iv). These results are consistent with the fact that Tsc13p is sequestered into NV junctions from the surrounding ER as *NVJ1* levels rise (Figures 1A and 2C). We conclude that the physiological up-regulation of Nvj1p during nutrient depletion promotes the targeting of microsomal Tsc13p into PMN structures, which likely leads to its degradation in the vacuole lumen.

De Novo Fatty Acid Synthesis and Elongation Are Required for the Normal Biogenesis of PMN Blebs and Vesicles

The targeting of Tsc13p into NV junctions and PMN structures raised the intriguing possibility that VLCFAs might play structural or functional roles during the rather complicated process of PMN. VLCFAs have been implicated in the maintenance of normal nuclear envelope structure in yeast and are thought to stabilize the lipid interface between the nuclear membrane and nuclear pore complexes (Schneiter *et al*., 1996). We were interested in determining whether Tsc13p activity (i.e., VLCFA biosynthesis) was necessary for PMN in starving cells. To this end, we investigated the effects of cerulenin, a specific inhibitor of FAS, on PMN. Cerulenin inhibits the de novo synthesis of medium-chain (C_{14}) and long-chain (C_{16}, C_{18}) fatty acids, which prime VLCFA synthesis (Awaya *et al*., 1975; Rossler *et al*., 2003). Additionally, high doses of cerulenin have been reported to impair VLCFA biosynthesis early in the microsomal fatty acid elongation cycle (Schneider *et al*., 1993; Evenson and Post-Beittenmiller, 1995). Using cerulenin, we tested whether the decreased availability of fatty acid substrates for Tsc13p could influence the biogenesis of PMN structures.

The effects of cerulenin on NV-junction formation and PMN morphology were analyzed in starving cells expressing integrated versions of *NVJ1-EYFP* and *TSC13-EGFP* under the control of their native promoters. NV junctions and PMN structures normally increase in size during nitrogen starvation as a consequence of the natural up-regulation of *NVJ1* expression in response to nutritional stress (Gasch *et al*., 2000; Roberts *et al*., 2003). Hence, both cTsc13p-EGFP and cNvj1p-EYFP localized to sizeable NV junctions and PMN blebs and vesicles in mock-treated cells after overnight starvation in SD-N (Figure 4, A and B). However, PMN structures seemed strikingly undersized in cells starved in the presence of cerulenin (Figure 4, A and B). Moreover, cTsc13p-EGFP, which strongly accumulated at NV junctions after acute starvation in mock-treated cells, seemed poorly localized to NV junctions in the presence of cerulenin (Figure 4A). Here, a significant portion of cTsc13p-EGFP localized outside of NV junctions to the surrounding perinuclear ER (Figure 4A). Cerulenin, on the other hand, had no effect on the proper localization of cNvj1p-EYFP to NV junctions (Figure 4B), indicating that the structural integrity of NV junctions was not significantly perturbed by the drug. These results establish a correlation between the inefficient targeting of cTsc13p-EGFP to NV junctions and the stunted appearance of PMN structures in cerulenin-treated cells. Importantly, supplementing the starvation medium with myristic acid (C_{14}), which bypasses the inhibitory effect of cerulenin (Awaya *et al*., 1975), completely restored the targeting of cTsc13p-EGFP to NV junctions and enlarged the size of PMN structures in cerulenin-treated cells (Figure 4, A and B). These results support a model in which fatty acid precursors of VLCFA biosynthesis mediate the proper targeting of Tsc13p to NV junctions and the biogenesis of PMN blebs and vesicles.

The notion that cerulenin reduces VLCFA levels in starved cells by perturbing fatty acid elongation was confirmed by acid methanolysis and gas chromatography of whole cell lipids (see *Materials and Methods*). Compared with control cells, cerulenin-treated cells exhibited 5-fold and 35-fold declines in the levels of C_{16} and C_{18} saturated fatty acids, respectively (Table 2). Concomitantly, C_{26} VLCFA pools were reduced more than 2.5-fold, and C_{20}, C_{22}, and C_{24} intermediate VLCFA-species became undetectable in cerulenin-treated cells (Table 2). In contrast, the levels of unsaturated fatty acids ($C_{16:1}$ and $C_{18:1}$) were unchanged or slightly elevated in cerulenin-treated compared with control cells (Table 2). Significantly, the populations of all long-chain and very-long-chain fatty acids were restored to near wt levels in cerulenin-treated cells that were supplemented with myristic acid (C_{14}) in order to bypass the cerulenin-induced block in FAS-catalyzed de novo fatty acid synthesis (Table 2).

Normally, VLCFAs produced by the microsomal fatty acid elongation cycle are fused with sphingoid bases to generate ceramides and sphingolipids (reviewed in Dickson, 1998). Thus, the stunted appearance of PMN structures in

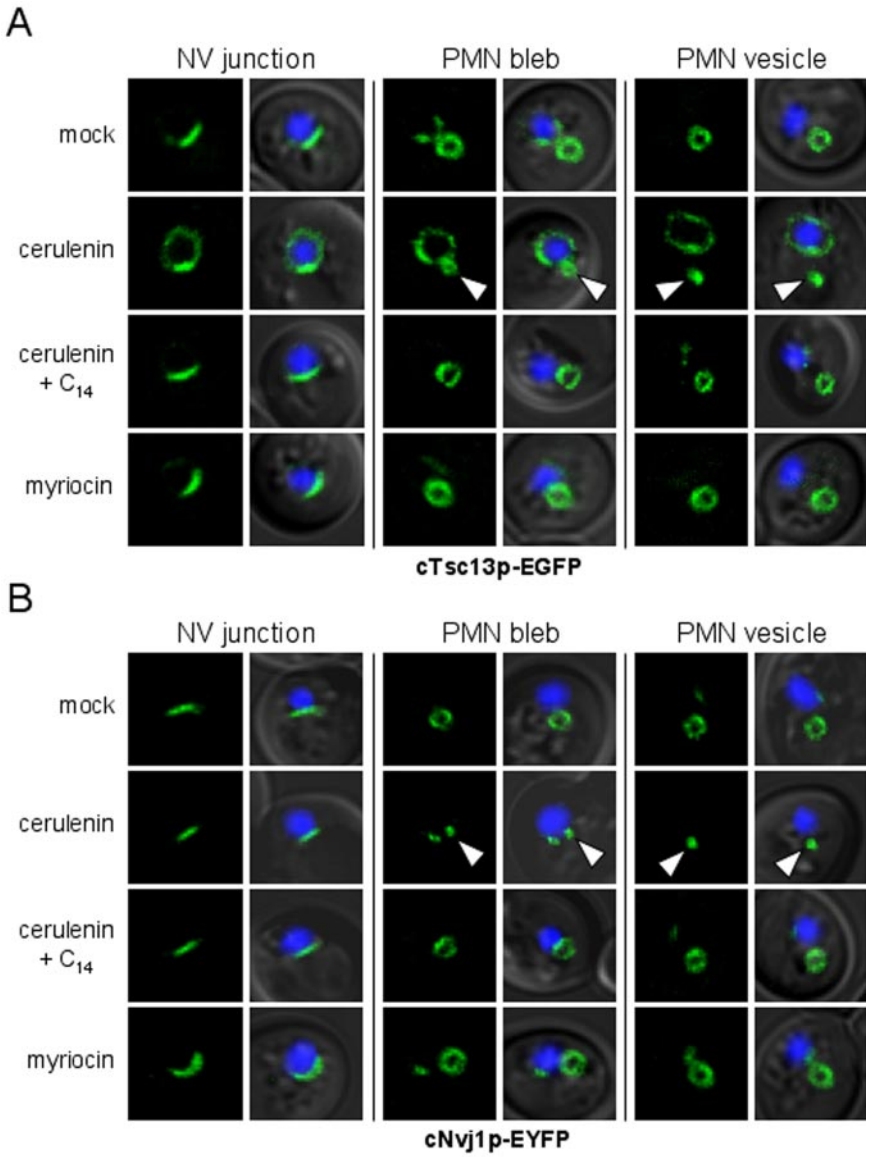

Figure 4. Cerulenin perturbs the targeting of Tsc13p to NV junctions and stunts PMN morphology in starved cells. (A and B) Localization of chromosomally expressed cTsc13p-EGFP (A) or cNvj1p-EYFP (B) to NV junctions and PMN blebs or vesicles in cells starved overnight in the presence or absence of cerulenin, myristic acid, or myriocin (see *Materials and Methods*). Nuclear chromatin (blue) was stained with Hoechst to reveal the position of nuclei in the overlays. Arrowheads point to stunted PMN blebs and vesicles in cerulenin-treated cells as revealed by both cTsc13p-EGFP (A) and cNvj1p-EYFP (B) fluorescence. Furthermore, cTsc13p-EGFP, which normally accumulates at NV junctions in starving cells treated with ethanol (A), looks delocalized from NV junctions in cerulenin-treated cells but reaccumulates at NV junctions upon supplementation with myristic acid (C_{14}). In contrast, cNvj1p-EYFP localizes strictly to NV junctions after all treatments (B). PMN structures in myriocin-treated cells or cerulenin-treated cells incubated with myristic acid (C_{14}) are of similar size and shape as mock-treated cells.

cerulenin-treated cells might be a consequence of perturbed ceramide and/or sphingolipid biosynthesis. To test this hypothesis, we analyzed the localization of cNvj1p-EYFP and cTsc13p-EGFP in cells starved and treated with myriocin (ISP-1), a potent inhibitor of fungal and mammalian serine palmitoyltransferases, which catalyze the first step of ceramide and sphingolipid synthesis (Miyake *et al*., 1995; Hanada, 2003). As shown in Figure 4, A and B, myriocin-treated cells exhibited normal PMN morphology, because both cNvj1p-EYFP and cTsc13p-EGFP localized to PMN structures of comparable size and shape to mock-treated cells. Moreover, cTsc13p-EGFP maintained a strong localization to NV junctions in myriocin-treated cells, in stark contrast to the affects of cerulenin (Figure 4A). The concentration of myriocin used in these experiments was sufficient to arrest cell growth in rich media, consistent with an inhibition of the cell's essential serine palmitoyltransferase activity (our unpublished data). Therefore, the observed effect of cerulenin on PMN morphology is unlikely to be a consequence of impaired ceramide and sphingolipid biosynthesis. Rather, these data support the notion that Tsc13p-catalyzed VLCFAs specifically contribute to PMN biogenesis.

Vac8p Retains an Acylation-dependent Association with Membranes in Cerulenin-treated Cells

Cerulenin is known to affect the acylation of some membrane-associated proteins by specifically inhibiting the protein acylation reaction (Lawrence *et al*., 1999). Both myristoylation and palmitoylation are critically important for the association of Vac8p with the vacuolar membrane (Wang *et al*., 1998). Therefore, it is possible that the effect of cerulenin on the size of PMN structures as well as the delocalization of cTsc13p-EGFP from NV junctions could be a consequence of deacylation and mislocalization of Vac8p to the cytosol. Using published Vac8p fractionation protocols (Wang *et al*., 1998; see *Materials and Methods*), we assessed the acylation-dependent association of Vac8p to the vacuole membrane in cells that were starved in the presence or absence of cerulenin. As shown in Figure 5A, little to no Vac8p was detected in soluble fractions (S100) of extracts from either cerulenin-

Table 2. Fatty acid profile of starved and treated cells

Fatty acid	Fatty acid composition (%)[a]			
	Mock	Cerulenin	Mock + C_{14}	Cerulenin + C_{14}
C_{14}	0.17 ± 0.01	0	NA	NA
$C_{14:1}$	0	0.21 ± 0.19	0.53 ± 0.08	0.63 ± 0.02
C_{16}	27.3 ± 1.2	1.06 ± 0.12	30.6 ± 1.8	36.4 ± 1.5
$C_{16:1}$	45.3 ± 1.5	76.4 ± 0.42	46.9 ± 1.2	51.7 ± 1.7
C_{18}	3.61 ± 0.09	0.78 ± 0.15	2.38 ± 0.11	1.97 ± 0.18
$C_{18:1}$	22.3 ± 0.46	20.3 ± 0.45	18.3 ± 1.6	8.21 ± 0.67
C_{20}	0.08 ± 0.04	0	0.05 ± 0.02	0.05 ± 0.03
C_{22}	0.07 ± 0.04	0	0.19 ± 0.15	0.03 ± 0.03
C_{24}	0.08 ± 0.01	0	0.05 ± 0.01	0.03 ± 0.02
C_{26}	1.01 ± 0.02	0.39 ± 0.04	0.77 ± 0.02	0.70 ± 0.03
Others	0.11 ± 0.09	0.77 ± 0.48	0.17 ± 0.02	0.24 ± 0.05

[a] Steady-state fatty acid compositions of starved cells treated with or without cerulenin and/or myristic acid (C_{14}) were determined as described in *Materials and Methods*. The amount of each fatty acid species was divided by the total population of fatty acid methyl esters and expressed as a percentage. Values represent the average fatty acid content and SD from three independent experiments and may not add up to 100% due to rounding. Note: C_{14} fatty acid methyl esters were excluded from the calculation when myristic acid was supplemented to the starvation medium because the absorption of external C_{14} on the cell surface cannot be excluded (Kohlwein and Paltauf, 1984).

treated or mock-treated cells, whereas the bulk of the cellular Vac8p pool fractionated with membranes (P13 and P100). In parallel, a Vac8p mutant protein lacking myristoylation and palmitoylation sites (*vac8-4*) was enriched in soluble fractions (S100), presumably due to its impaired ability to associate with membranes (Figure 5A) (Wang *et al*., 1998).

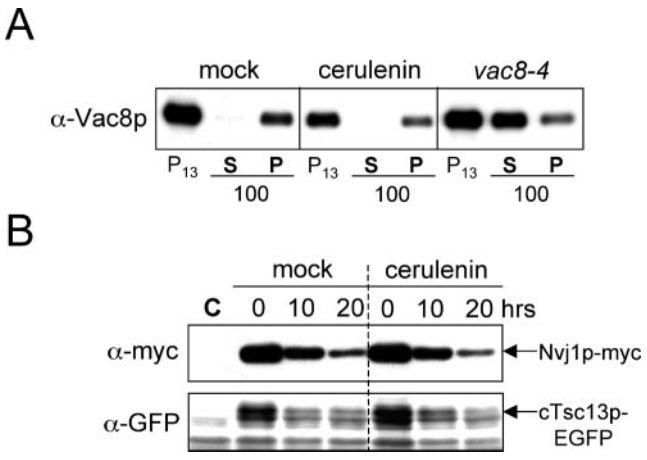

Figure 5. Vac8p membrane association as well as PMN-mediated protein turnover are normal in the presence of cerulenin. (A) Vac8p efficiently fractionates with isolated membranes in cells starved in the presence or absence of cerulenin. Whole cell extracts were fractionated by differential centrifugation as described in *Materials and Methods*. As a control, *vac8-4* cells (expressing a mutant form of Vac8p lacking myristoylation and palmitoylation sites) were fractionated in a similar manner. Vac8p was detected in isolated membrane fractions (P13 and P100) but not soluble fractions (S100) of extracts from mock-treated and cerulenin-treated cells. (B) The starvation-induced degradation of Nvj1p-myc and cTsc13p-EGFP is normal in the presence of cerulenin. A "pulse" of Nvj1p-myc was expressed in wt cells harboring P_{GAL1}-*NVJ1-myc*, and its degradation was analyzed after glucose-induced repression in nitrogen starvation media, which was supplemented with cerulenin or ethanol (see *Materials and Methods*). The expression of cTsc13p-EGFP was controlled from the *TSC13* chromosomal locus. Wild-type control extract denoted as C.

Therefore, cerulenin failed to significantly affect the association of Vac8p with the vacuole membrane. We conclude that the effect of cerulenin on the size of PMN blebs and vesicles is not due to a reduction in the level of vacuole-associated Vac8p. This conclusion is supported by the observation that the strict localization of Nvj1p-EYFP to perinuclear ER patches, which is mediated by heterotropic interactions with Vac8p, was not affected by cerulenin treatment (Figure 4B).

PMN-mediated Protein Turnover Is Normal in Cerulenin-treated Cells

Due to the shrunken appearance of PMN structures in the presence of cerulenin (Figure 4, A and B), we next tested whether cerulenin impaired PMN-mediated protein turnover during starvation. Using previously described biochemical assays for PMN (Kvam and Goldfarb, 2004), we assessed the degradation rate of an Nvj1p-myc reporter in the presence and absence of cerulenin (see *Materials and Methods*). Surprisingly, immunoblot analysis revealed that the turnover of Nvj1p-myc was equally efficient in cerulenin-treated cells as mock-treated cells over a 20-h starvation time course (Figure 5B). Thus, cerulenin failed to perturb the overall rate of PMN-mediated protein degradation despite its striking effect on the size of PMN structures. These results were corroborated by monitoring the starvation-induced degradation of cTsc13p-EGFP after cerulenin treatment (Figure 5B). From these data, we conclude that rates of PMN throughput are apparently not dependent on the sizes of PMN blebs and vesicles.

PMN Morphology Is Significantly Altered in VLCFA Elongation Mutants

Our cerulenin experiments suggest a role for Tsc13p and VLCFAs in the biogenesis of PMN blebs and vesicles. To assess this role more directly, we analyzed the morphology of PMN structures in a *tsc13-1* mutant encoding a lysine substitution at a conserved glutamine residue (Q81K) that is shared among several Tsc13p homologues including human and mouse *trans*-2,3-enoyl-CoA reductases (Kohlwein *et al*., 2001; Moon and Horton, 2003). This *tsc13-1* allele was identified in a suppressor screen for yeast mutants defective in

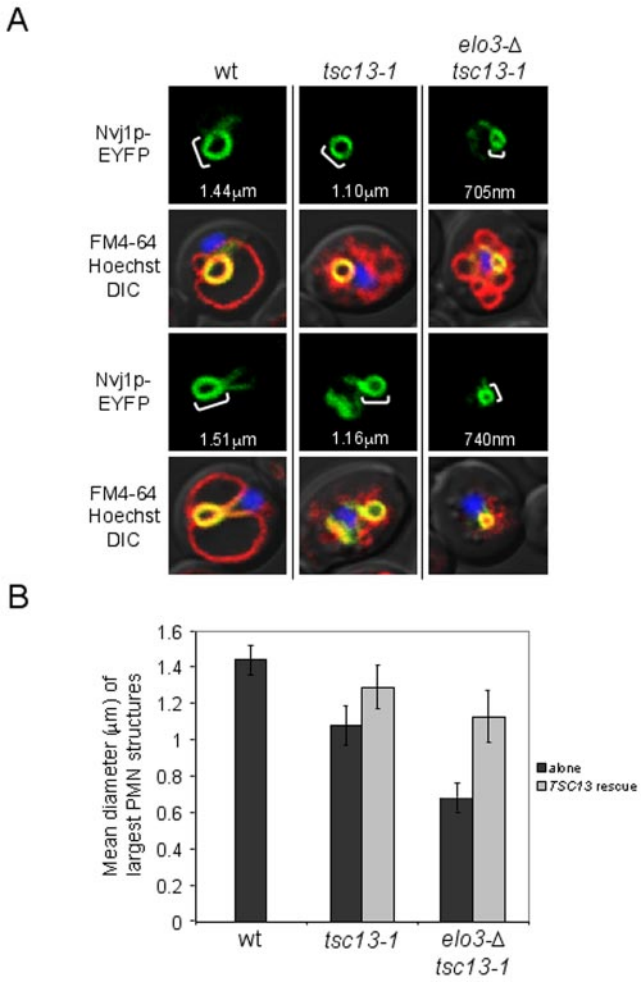

Figure 6. PMN morphology is significantly altered in VLCFA elongation mutants. (A) The size and lumenal diameter of PMN blebs and vesicles are significantly undersized in *tsc13-1* and *elo3*-Δ *tsc13-1* fatty acid elongation mutants during starvation. PMN morphology was analyzed in *tsc13-1*, *elo3*-Δ *tsc13-1*, and their wt parental strain (TDY2037) using P_{CUP1}-*NVJ1-EYFP* as a reporter. Cells were grown to ~0.1 OD_{600} and starved in SD-N for 3.5 h before confocal imaging. Vacuolar membranes (red) and nuclear chromatin (blue) were stained with FM4-64 and Hoechst, respectively, and superimposed. PMN diameters were measured using the Profile function of the confocal software (see *Materials and Methods*). (B) The mean diameters of *tsc13-1* and *elo3*-Δ *tsc13-1* PMN structures are statistically and incrementally smaller than wt cells but become enlarged upon the introduction of plasmid-encoded *TSC13*. Lumenal diameters (micrometers) of the largest representative PMN structures were measured in 10–15 cells from starving wt, *tsc13-1*, and *elo3*Δ *tsc13-1* cultures, respectively, using the Profile function of the confocal software (see *Materials and Methods*). Cells were cultured, labeled, and starved as described in A. These experiments were then repeated in *tsc13-1* and *elo3*Δ *tsc13-1* cells harboring pRS425-*TSC13*, and the values were averaged.

sphingolipid synthesis and accounts for an ~50% reduction in fatty acid elongation activity in vitro (Kohlwein *et al*., 2001). PMN morphology was analyzed in starved *tsc13-1* cells using inducible P_{CUP1}-*NVJ1-EYFP* as a reporter. By confocal microscopy, PMN structures in *tsc13-1* cells looked smaller than those in the parental wt strain (Figure 6A). The *tsc13-1* mutant also stained poorly with FM4-64 vacuole stain and exhibited multilobed or fragmented vacuoles similar to other mutants in the VLCFA biosynthetic pathway (Kohlwein *et al*., 2001). Codisruption of the microsomal fatty acid elongase *ELO3* in *tsc13-1* cells further reduced the average size of PMN blebs and vesicles during starvation (Figure 6A). Western blot analyses confirmed that Nvj1p-EYFP was expressed equally among these strains (our unpublished data). We measured and compared the lumenal diameters of PMN blebs and vesicles in samples of wt, *tsc13-1*, and *elo3*Δ *tsc13-1* mutant cells (see *Materials and Methods*). As shown in Figure 6B, PMN structures in both *tsc13-1* and *elo3*Δ *tsc13-1* cells were statistically smaller than those in wt cells (Figure 6B). Because *elo3*Δ *tsc13-1* cells exhibited similar vacuole morphology defects as *tsc13-1* mutants alone, it is unlikely that the progressive decline in size of PMN structures between these mutants can be explained by changes in vacuole structure. Importantly, the introduction of a plasmid-encoded copy of *TSC13* under the transcriptional control of its endogenous promoter largely rescued normal PMN size phenotypes in *tsc13-1* and *elo3*-Δ *tsc13-1* cells (Figure 6B). Together, these data strongly implicate de novo VLCFA biosynthesis in the formation of PMN blebs and vesicles. In total, our experiments demonstrate that the selective targeting of Tsc13p to NV junctions and the compartmentalized biosynthesis of VLCFAs play important roles in the biogenesis of nuclear blebs and vesicles during PMN.

DISCUSSION

Nvj1p is an integral membrane protein of the outer nuclear membrane that creates a platform for the assembly of a unique subdomain of the perinuclear ER membrane. We previously reported that Nvj1p binds and recruits the vacuolar membrane-associated protein Vac8p, which gives rise to Velcro-like interorganelle junctions between the nucleus and vacuole (Pan *et al*., 2000). Nvj1p also binds and sequesters the oxysterol-binding protein homolog Osh1p, which is targeted to NV junctions from cytosolic and Golgi pools (Levine and Munro, 2001; Kvam and Goldfarb, 2004). In this study, we show that the accumulation of Tsc13p at NV junctions, first reported by Kohlwein *et al*. (2001), is mediated by a physical interaction with Nvj1p. As in the cases of Osh1p and Vac8p, the localization of Tsc13p to NV junctions is dependent on Nvj1p, and its sequestration into NV junctions is directly proportional to *NVJ1* expression levels. Moreover, we demonstrate that Nvj1p binds and recruits Tsc13p to the perinuclear ER from surrounding ER compartments even in cells lacking Vac8p and NV junctions. Therefore, the vacuole membrane is not required for the sequestration of Tsc13p into Nvj1p-enriched subdomains of the perinuclear ER.

The enrichment of both Tsc13p and Osh1p at NV junctions is reminiscent of the accumulation of factors involved in lipid biochemistry at other ER contact sites (Stone and Vance, 2000; Pichler *et al*., 2001). Studies of these contact sites suggest that interorganelle molecular junctions might be a general property of most ER contact sites (reviewed in Levine, 2004). However, the Velcro-like Vac8p-Nvj1p interaction is the only known interorganelle junction-forming apparatus. Uniquely, NV junctions are also platforms for the PMN, during which portions of the nucleus are pinched off into the vacuole lumen and degraded. Because NV junctions strictly define the portion of the nuclear envelope engulfed by the invaginating vacuole membrane, Nvj1p and all three of its known binding partners (Vac8p, Tsc13p, and Osh1p)—and other associated proteins or lipids—must be delivered by PMN into the hydrolytic vacuole lumen.

Because Nvj1p expression levels are tightly coupled to the formation and proliferation of NV junctions and PMN, the Nvj1p-dependent targeting of Tsc13p to NV junctions is spatially and temporally correlated with PMN biogenesis. In addition to demonstrating a physical interaction between Tsc13p and Nvj1p, we present three lines of evidence in support a functional relationship between the targeting of Tsc13p to NV junctions and the biogenesis of PMN vesicles. First, morphometric analyses demonstrate that the lumenal diameters of PMN structures are significantly smaller in *tsc13-1* and *elo3*-Δ *tsc13-1* fatty acid elongation mutants compared to wt cells. Second, PMN blebs and vesicles are strikingly smaller in starved cells after treatment with cerulenin, an inhibitor of de novo fatty acid synthesis and elongation. Last, cerulenin promotes the marked delocalization of Tsc13p-EGFP from NV junctions in starved cells, which suggests that a continuous supply of fatty acid substrates may be required for the proper targeting of Tsc13p to NV junctions. Both consequences of cerulenin treatment (i.e., the stunting of PMN structures and the mistargeting of Tsc13p-EYFP from NV junctions) are suppressed by feeding the cells with myristic acid, which bypasses the cerulenin-induced block in de novo fatty acid synthesis. These observations suggest that the enzymatic activity of Tsc13p during VLCFA biosynthesis contributes to the biogenesis of PMN blebs and vesicles at NV junctions.

The delocalization of Tsc13p-EGFP from NV junctions in the presence of cerulenin is interesting because it links the enzyme's localization to the supply of its fatty acid substrates. By analogy, the localization of yeast acyl chain desaturase, Ole1p, was reported to shift from a uniform ER distribution to punctate domains along the cell periphery in a substrate-dependent manner (Tatzer *et al*., 2002). Because Tsc13p physically associates with Elo2p and Elo3p fatty acid elongases (Kohlwein *et al*., 2001), the substrate-dependent localization of Tsc13p to NV junctions implies that active elongation complexes may transiently assemble at NV junctions. Thus, distinct elongation complexes containing Tsc13p are likely required for the normal biogenesis of PMN blebs and vesicles. In support of this, we determined that additional enzymes of the microsomal VLCFA elongation system (Elo2p, Elo3p, and YBR159p) are present, but not concentrated, within NV junctions. Moreover, the lumenal diameters of PMN structures are significantly smaller in *elo3*-Δ *tsc13-1* cells than *tsc13-1* cells alone.

Despite the dramatic effects of cerulenin on the size of PMN blebs and vesicles, cerulenin showed no significant effects on PMN-mediated protein turnover during starvation. This observation demonstrates that the rate of PMN throughput is not necessarily proportional to the size of PMN intermediates. Wild-type rates of PMN are probably maintained in the presence of cerulenin through the formation of many small and/or unstable PMN blebs and vesicles. Under these conditions, the scission of PMN blebs into the vacuole lumen may occur faster than normal due to structural instabilities in the membrane architecture of PMN blebs. Alternatively, we cannot rule out the possibility, however unlikely, that components of NV junctions may be degraded by other proteolytic systems under these conditions. This issue deserves more study because the packaging of some nuclear constituents into PMN vesicles, such as the granular nucleolus, might be affected by altering the size of PMN blebs.

Previously, we reported that cells depleted of the entire oxysterol-binding protein family (Osh1p-Osh7p) accumulate PMN intermediates, consistent with the idea that sterol lipid homeostasis is required for the proper formation of mature blebs and vesicles (Kvam and Goldfarb, 2004). In addition to sterol lipids, our present study suggests a role for VLCFA-containing lipids at NV junctions. Several studies in yeast have highlighted an importance for VLCFA synthesis in membrane structure and vesicular trafficking. For example, VLCFA synthesis is integral to the structure of the yeast nuclear envelope (Schneiter *et al*., 1996) as well as for vacuole assembly and fusion (Faergeman *et al*., 2004). Spontaneous mutations in either of the yeast VLCFA elongases *ELO2* or *ELO3* bypass the requirement for vesicular soluble *N*-ethylmaleimide sensitive factor attachment protein receptors during secretion (David *et al*., 1998). VLCFAs are proposed to facilitate these roles by promoting the formation of highly curved membrane structures (reviewed in Schneiter and Kohlwein, 1997). In model membranes, VLCFA-substituted lipids have been shown to perturb bilayer structure and facilitate membrane curvature due to their extended hydrophobic tails (Schneiter and Kohlwein, 1997). Thus, deficiencies in VLCFA-substituted lipids are associated with circumstances of membrane hyper-rigidity, such as restrictive dermopathy in mammals (Herrmann *et al*., 2003). Based on these observations, we propose that VLCFAs may be required for the efficient biogenesis of highly curved blebs and vesicles during the process of PMN. It is important to note that PMN blebs and vesicles are comprised of three concentric membranes, namely, the vacuole membrane and the double-membrane nuclear envelope, which pose unusual constraints on their biogenesis.

Interestingly, myriocin, which inhibits the biosynthesis of ceramides and sphingolipids, failed to alter PMN morphology in starving cells. These data imply that VLCFAs alone, or VLCFA-containing lipids other than ceramides and sphingolipids, play a specific role during PMN. By analogy to the role of sphingolipids in the partitioning of membrane proteins into lipid rafts (reviewed in Salaun *et al*., 2004), the accumulation of VLCFAs and/or VLCFA-containing lipids in NV junctions could serve to facilitate the partitioning of Nvj1p and associated binding partners (including Tsc13p itself) into NV junctions. However, this model does not exclude a role for ceramides or sphingolipids in the biology of NV junctions, because, in the presence of myriocin, these VLCFA-containing lipids could be recruited into NV junctions from preexisting pools. Rather, our results are consistent with the more general idea that the lipid composition of NV junctions is modified by Tsc13p (and the microsomal VLCFA elongation system) preceding or following the formation of nascent PMN blebs and that this lipid environment contributes to normal PMN biogenesis.

The Nvj1p-mediated targeting of Tsc13p to NV junctions could pose other physiological consequences for the cell. For example, the sequestration of Tsc13p away from peripheral ER pools is likely to reduce the rate of local VLCFA biosynthesis in other subcellular ER compartments, which could have a variety of effects on bulk membrane biology. The degradation of NV junction-associated Tsc13p during PMN may also affect the general rate of VLCFA biosynthesis in the cell during starvation. Because VLCFA-containing lipids are required for vacuole biogenesis and fusion (Faergeman *et al*., 2004), their production in the perinuclear ER at NV junctions could provide a ready source of lipids for vacuole compartments.

In conclusion, this study demonstrates that Nvj1p binds and sequesters Tsc13p, an essential enoyl-CoA reductase in the microsomal fatty acid elongation system, into NV junctions through a mechanism directly analogous to the Nvj1p-mediated targeting of Vac8p and Osh1p (Kvam and Goldfarb, 2004; Pan *et al*., 2000). By analogy to other ER

membrane contact sites, these findings support a role for Nvj1p in the organization of a specialized domain of the nuclear ER that mediates PMN. Our results argue most strongly that Tsc13p plays a compartmentalized role in the biogenesis of PMN structures, and that VLCFA-containing lipids contribute to the production of these trilaminar structures. However, by analogy to the utility of ER-mitochondria contact sites in the interorganellar trafficking of phospholipids, it is also possible that the targeting of Tsc13p and Osh1p to NV junctions may function in general lipid metabolism and homeostasis. Further work is needed to distinguish among these interrelated models.

ACKNOWLEDGMENTS

We thank Xiaoyuan Song for technical assistance with plasmid construction, Sepp Kohlwein for pUG35-*ELO2-EGFP*, and Lois Weisman for the *vac8-4* plasmid. This study was supported by National Institutes of Health Grant (R01 GM-67838 (to D.S.G.) and National Science Foundation Grants MCB 0110972 (to D.S.G.) MCB 0313466 (to T.MD.).

REFERENCES

Achleitner, G., Gaigg, B., Krasser, A., Kainersdorfer, E., Kohlwein, S. D., Perktold, A., Zellnig, G., and Daum, G. (1999). Association between the endoplasmic reticulum and mitochondria of yeast facilitates interorganelle transport of phospholipids through membrane contact. Eur. J. Biochem. *264*, 545–553.

Awaya, J., Ohno, T., Ohno, H., and Omura, S. (1975). Substitution of cellular fatty acids in yeast cells by the antibiotic cerulenin and exogenous fatty acids. Biochim. Biophys. Acta *409*, 267–273.

Bi, E., and Pringle, J. R. (1996). ZDS1 and ZDS2, genes whose products may regulate Cdc42p in *Saccharomyces cerevisiae*. Mol. Cell. Biol. *16*, 5264–5275.

Boukh-Viner, T., *et al*. (2005). Dynamic ergosterol- and ceramide-rich domains in the peroxisomal membrane serve as an organizing platform for peroxisome fusion. J. Cell Biol. *168*, 761–773.

David, D., Sundararabu, S., and Gerst, J. E. (1998). Involvement of long chain fatty acid elongation in the trafficking of secretory vesicles in yeast. J. Cell Biol. *143*, 1167–1182.

Dickson, R. C. (1998). Sphingolipid functions in *Saccharomyces cerevisiae*: comparison to mammals. Annu. Rev. Biochem. *67*, 27–48.

Dupre, S., and Haguenauer-Tsapis, R. (2003). Raft partitioning of the yeast uracil permease during trafficking along the endocytic pathway. Traffic *4*, 83–96.

Eisenkolb, M., Zenzmaier, C., Leitner, E., and Schneiter, R. (2002). A specific structural requirement for ergosterol in long-chain fatty acid synthesis mutants important for maintaining raft domains in yeast. *13*, 4414–4428.

Evenson, K. J., and Post-Beittenmiller, D. (1995). Fatty acid-elongating activity in rapidly expanding leek epidermis. Plant Physiol. *109*, 707–716.

Faergeman, N. J., Feddersen, S., Christiansen, J. K., Larsen, M. K., Schneiter, R., Undermann, C., Mutenda, K., Roepstorff, P., and Knudsen, J. (2004). Acyl-CoA-binding protein, Acb1p, is required for normal vacuole function and ceramide synthesis in *Saccharomyces cerevisiae*. Biochem. J. *380*, 907–918.

Gable, K., Garton, S., Napier, J. A., and Dunn, T. M. (2004). Functional characterization of the *Arabidopsis thaliana* orthologue of Tsc13p, the enoyl reductase of the yeast microsomal fatty acid elongating system. J. Exp. Bot. *55*, 543–545.

Gaigg, B., Simbeni, R., Hrastnik, C., Paltauf, F., and Daum, G. (1995). Characterization of a microsomal subfraction associated with mitochondria of the yeast *Saccharomyces cerevisiae*. Involvement in synthesis and import of phospholipids into mitochondria. Biochim. Biophys. Acta *1234*, 214–220.

Gasch, A. P., Spellman, P. T., Kao, C. M., Carmel-Harel, O., Eisen, M. B., Storz, G., Botstein, D., and Brown, P. O. (2000). Genomic expression programs in the response of yeast cells to environmental changes. Mol. Biol. Cell *11*, 4241–4257.

Han, G., Gable, K., Kohlwein, S. D., Beaudoin, F., Napier, J. A., and Dunn, T. M. (2002). The *Saccharomyces cerevisiae* YBR159w gene encodes the 3-ketoreductase of the microsomal fatty acid elongase. J. Biol. Chem. *277*, 35440–35449.

Hanada, K. (2003). Serine palmitoyltransferase, a key enzyme of sphingolipid metabolism. Biochim. Biophys. Acta *1632*, 16–30.

Hanada, K., Kumagai, K., Yasuda, S., Miura, Y., Kawano, M., Fukasawa, M., and Nishijima, M. (2003). Molecular machinery for non-vesicular trafficking of ceramide. Nature *426*, 803–809.

Herrmann, T., *et al*. (2003). Mice with targeted disruption of the fatty acid transport protein 4 (Fatp 4, Slc27a4) gene show features of lethal restrictive dermopathy. J. Cell Biol. *161*, 1105–1115.

Ho, J. K., Moser, H., Kishimoto, Y., and Hamilton, J. A. (1995). Interactions of a very long chain fatty acid with model membranes and serum albumin. Implications for the pathogenesis of adrenoleukodystrophy. J. Clin. Investig. *96*, 1455–1463.

Kim, J., Dalton, V. M., Eggerton, K. P., Scott, S. V., and Klionsky, D. J. (1999). Apg7p/Cvt2p is required for the cytoplasm-to-vacuole targeting, macroautophagy, and peroxisome degradation pathways. Mol. Biol. Cell *10*, 1337–1351.

Kohlwein, S. D., and Paltauf, F. (1984). Uptake of fatty acids by the yeasts, *Saccharomyces uvarum* and *Saccharomyces lipolytica*. Biochim. Biophys. Acta *792*, 310–317.

Kohlwein, S. D., Eder, S., Oh, C. S., Martin, C. E., Gable, K., Bacikova, D., and Dunn, T. (2001). Tsc13p is required for fatty acid elongation and localizes to a novel structure at the nuclear-vacuolar interface in *Saccharomyces cerevisiae*. Mol. Cell. Biol. *21*, 109–125.

Kumagai, K., Yasuda, S., Okemoto, K., Nishijima, M., Kobayashi, S., and Hanada, K. (2005). CERT mediates intermembrane transfer of various molecular species of ceramides. J. Biol. Chem. *280*, 6488–6495.

Kvam, E., and Goldfarb, D. S. (2004). Nvj1p is the outer-nuclear-membrane receptor for oxysterol-binding protein homolog Osh1p in *Saccharomyces cerevisiae*. J. Cell Sci. *117*, 4959–4968.

Lawrence, D. S., Zilfou, J. T., and Smith, C. D. (1999). Structure-activity studies of cerulenin analogues as protein palmitoylation inhibitors. J. Med. Chem. *42*, 4932–4941.

Levine, T. (2004). Short-range intracellular trafficking of small molecules across endoplasmic reticulum junctions. Trends Cell Biol. *14*, 483–490.

Levine, T. P., and Munro, S. (2001). Dual targeting of Osh1p, a yeast homologue of oxysterol-binding protein, to both the Golgi and the nucleus-vacuole junction. Mol. Biol. Cell *12*, 1633–1644.

Macreadie, I. G., Jagadish, M. N., Azad, A. A., and Vaughan, P. R. (1989). Versatile cassettes designed for the copper inducible expression of proteins in yeast. Plasmid *21*, 147–150.

Millar, A. A., Wrischer, M., and Kunst, L. (1998). Accumulation of very-long-chain fatty acids in membrane glycerolipids is associated with dramatic alterations in plant morphology. Plant Cell *10*, 1889–1902.

Miyake, Y., Kozutsumi, Y., Nakamura, S., Fujita, T., and Kawasaki, T. (1995). Serine palmitoyltransferase is the primary target of a sphingosine-like immunosuppressant, ISP-1/myriocin. Biochem. Biophys. Res. Commun. *211*, 396–403.

Moon, Y. A., and Horton, J. D. (2003). Identification of two mammalian reductases involved in the two-carbon fatty acyl elongation cascade. J. Biol. Chem. *278*, 7335–7343.

Moskvina, E., Schuller, C., Maurer, C. T., Mager, W. H., and Ruis, H. (1998). A search in the genome of *Saccharomyces cerevisiae* for genes regulated via stress response elements. Yeast *14*, 1041–1050.

Oh, C. S., Toke, D. A., Mandala, S., and Martin, C. E. (1997). ELO2 and ELO3, homologues of the *Saccharomyces cerevisiae* ELO1 gene, function in fatty acid elongation and are required for sphingolipid formation. J. Biol. Chem. *272*, 17376–17384.

Pan, X., and Goldfarb, D. S. (1998). YEB3/VAC8 encodes a myristylated armadillo protein of the *Saccharomyces cerevisiae* vacuolar membrane that functions in vacuole fusion and inheritance. J. Cell Sci. *111*, 2137–2147.

Pan, X., Roberts, P., Chen, Y., Kvam, E., Shulga, N., Huang, K., Lemmon, S., and Goldfarb, D. S. (2000). Nucleus-vacuole junctions in *Saccharomyces cerevisiae* are formed through the direct interaction of Vac8p with Nvj1p. Mol. Biol. Cell *11*, 2445–2457.

Pichler, H., Gaigg, B., Hrastnik, C., Achleitner, G., Kohlwein, S. D., Zellnig, G., Perktold, A., and Daum, G. (2001). A subfraction of the yeast endoplasmic reticulum associates with the plasma membrane and has a high capacity to synthesize lipids. Eur. J. Biochem. *268*, 2351–2361.

Roberts, P., Moshitch-Moshkovitz, S., Kvam, E., O'Toole, E., Winey, M., and Goldfarb, D. S. (2003). Piecemeal microautophagy of the nucleus in *Saccharomyces cerevisiae*. Mol. Biol. Cell *14*, 129–141.

Rossler, H., Rieck, C., Delong, T., Hoja, U., and Schweizer, E. (2003). Functional differentiation and selective inactivation of multiple *Saccharomyces cerevisiae* genes involved in very-long-chain fatty acid synthesis. Mol. Genet. Genomics *269*, 290–298.

Rusinol, A. E., Cui, Z., Chen, M. H., and Vance, J. E. (1994). A unique mitochondria-associated membrane fraction from rat liver has a high capacity for lipid synthesis and contains pre-Golgi secretory proteins including nascent lipoproteins. J. Biol. Chem. *269*, 27494–27502.

Salaun, C., James, D. J., and Chamberlain, L. H. (2004). Lipid rafts and the regulation of exocytosis. Traffic *5*, 255–264.

Schneider, F., Lessire, R., Bessoule, J. J., Juguelin, H., and Cassagne, C. (1993). Effect of cerulenin on the synthesis of very-long-chain fatty acids in microsomes from leek seedlings. Biochim. Biophys. Acta *1152*, 243–252.

Schneiter, R., Hitomi, M., Ivessa, A. S., Fasch, E. V., Kohlwein, S. D., and Tartakoff, A. M. (1996). A yeast acetyl coenzyme A carboxylase mutant links very-long-chain fatty acid synthesis to the structure and function of the nuclear membrane-pore complex. Mol. Cell. Biol. *16*, 7161–7172.

Schneiter, R., and Kohlwein, S. D. (1997). Organelle structure, function, and inheritance in yeast: a role for fatty acid synthesis? Cell *88*, 431–434.

Sherman, F. (1991). Getting started with yeast. Methods Enzymol. *194*, 3–21.

Staehelin, L. A. (1997). The plant ER: a dynamic organelle composed of a large number of discrete functional domains. Plant J. *11*, 1151–1165.

Stone, S. J., and Vance, J. E. (2000). Phosphatidylserine synthase-1 and -2 are localized to mitochondria-associated membranes. J. Biol. Chem. *275*, 34534–34540.

Tatzer, V., Zellnig, G., Kohlwein, S. D., and Schneiter, R. (2002). Lipid-dependent subcellular relocalization of the acyl chain desaturase in yeast. Mol. Biol. Cell *13*, 4429–4442.

Voeltz, G. K., Rolls, M. M., and Rapoport, T. A. (2002). Structural organization of the endoplasmic reticulum. EMBO Rep. *3*, 944–950.

Wang, Y. X., Catlett, N. L., and Weisman, L. S. (1998). Vac8p, a vacuolar protein with armadillo repeats, functions in both vacuole inheritance and protein targeting from the cytoplasm to vacuole. J. Cell Biol. *140*, 1063–1074.

Welch, J. W., and Burlingame, A. L. (1973). Very long-chain fatty acids in yeast. J. Bacteriol. *115*, 464–466.